Synsint Research Group

Available online at www.synsint.com

Synthesis and Sintering

ISSN 2564-0186 (Print), ISSN 2564-0194 (Online)

Research article

Microstructural evolution and mechanical performance of TiO_2 nanoparticle-reinforced Fe_2O_3–Al reactive composites

Mostafa Pasban *, Ali Alizadeh, Hamid Reza Baharvandi

Faculty of Materials and Manufacturing Processes, Malek Ashtar University of Technology, Tehran, Iran

ABSTRACT

In this study, Fe_2O_3-Al reactive composite samples containing different concentrations of TiO_2 nanoparticles (0.1, 0.2, 0.3, 0.4, and 0.5 wt%) were prepared through ultrasonic mixing followed by thermite combustion in sand molds. Before nanoparticle incorporation, the optimum Fe_2O_3:Al ratio was determined as 3:1, which produced the highest iron yield (116.2 g) with a reaction time of 26.43 s, falling within the industrially desirable range of 23–28 s. X-ray diffraction (XRD) analysis revealed that the base sample primarily consisted of α-Fe and α-Al_2O_3 phases, while TiO_2-containing samples exhibited additional peaks associated with FeTi and Fe_2Ti intermetallic compounds. Field-emission scanning electron microscopy (FESEM) coupled with energy-dispersive spectroscopy (EDS) confirmed a uniform nanoparticle distribution up to 0.4 wt%, whereas noticeable agglomeration was observed at 0.5 wt%. Mechanical characterization demonstrated that the sample containing 0.4 wt% TiO_2 exhibited the highest density (7.81 g/cm^3, corresponding to a 21.7% increase), hardness (293 HV, 36.3% increase), tensile strength (665 MPa, 35.2% increase), and compressive strength (732 MPa, 18.6% increase). Furthermore, the maximum impact energy (265 J, representing a 61.6% increase) and the highest wear resistance (30% reduction in wear depth) were achieved at the same nanoparticle content. The observed improvements are attributed to combined strengthening mechanisms including grain refinement, Orowan strengthening, crack deflection, and thermal mismatch effects.

KEYWORDS

Thermite welding
TiO_2 nanoparticles
Reactive composites
FeTi intermetallic compounds
Mechanical properties
Grain refinement

OPEN ACCESS

1. Introduction

The relatively low strength and toughness of the weld zone remain major challenges in thermite rail welding applications. This limitation has motivated considerable research efforts aimed at improving the mechanical performance of thermite welds through the incorporation of alloying elements and reinforcing phases capable of refining the microstructure or reducing casting-related defects [1–3]. Although the addition of alloying elements has resulted in some improvements in mechanical performance, achieving simultaneous enhancement of strength and toughness remains a significant challenge [4, 5].

In recent years, nanoparticle incorporation has emerged as an effective approach for improving the mechanical properties of welded structures. Reducing particle dimensions to the nanoscale substantially increases the surface-area-to-volume ratio, resulting in stronger interactions with the surrounding metallic matrix [6, 7]. Furthermore, nanoparticles can serve as heterogeneous nucleation sites during solidification, leading to grain refinement and consequently improving both strength and toughness. Several studies have reported beneficial effects of nanoparticle additions on the microstructural and mechanical properties of welded joints [8]. However, the tendency of nanoparticles to agglomerate remains a major challenge because non-uniform dispersion can adversely affect the resulting properties.

* Corresponding author. *E-mail address:* mostafapaseban588@gmail.com (M. Pasban)

Received 22 June 2026; Received in revised form 22 July 2026; Accepted 22 July 2026.

https://doi.org/10.53063/synsint.2026.63356

Among the various reinforcing nanoparticles, titanium dioxide (TiO_2) is considered particularly attractive for improving weld microstructures and mechanical performance because of its high thermal stability, elevated melting point (1843 °C), and its ability to promote intragranular ferrite nucleation [9, 10]. Ramkumar and Natarajan [11] reported significant microstructural refinement and improved mechanical properties in gas tungsten arc welded Al3003 alloy joints containing TiO_2 nanoparticles. Similarly, previous studies involving electrode welds have demonstrated considerable increases in tensile strength and hardness following TiO_2 nanoparticle incorporation [12].

Beyond conventional arc welding applications, extensive studies have been conducted on Fe_2O_3- TiO_2-Al systems using various combustion synthesis approaches [13, 14]. Yeh and Ke [15] demonstrated that fine particles can hinder dislocation movement through the Orowan strengthening mechanism while simultaneously improving fracture toughness through crack deflection. However, excessive reinforcement content resulted in particle agglomeration and subsequent deterioration of mechanical performance.

Mousavian et al. [16] employed the heat generated from the Fe_2O_3-Al reaction as a localized thermal source to facilitate TiO_2 reduction kinetics, whereas mechanical activation increased the contact area between reactants, thereby enabling reaction completion at lower temperatures. Kobyakov and Kovalev [17] reported the formation of TiFe and $TiFe_2$ phases according to the Fe--Ti phase diagram. Li et al. [18] investigated ferrotitanium alloys prepared through solid-solution strengthening, while Meng et al. [19] utilized TiC as an interlayer material and achieved controlled phase separation through centrifugal processing. Wang et al. [20] proposed a melt-dispersion mechanism indicating that reducing particle size to the nanoscale significantly accelerates reaction kinetics. Mashayekh and Baharvandi [21] reported a transition in diffusion mechanisms from grain-boundary diffusion to volume diffusion and identified the formation of solid solutions as beneficial for improving material properties.

Although TiO_2 nanoparticles have been extensively investigated in conventional welding systems and combustion synthesis processes, their influence on thermite-derived Fe_2O_3-Al reactive composites remains largely unexplored. In particular, limited attention has been given to achieving simultaneous enhancement of strength and toughness through nanoparticle reinforcement under the rapid heating and solidification conditions associated with thermite processing. Therefore, the present study investigates the effects of different TiO_2 nanoparticle concentrations (0.1, 0.2, 0.3, 0.4, and 0.5 wt%) on the microstructural characteristics and mechanical properties of Fe_2O_3-Al reactive composites.

2. Materials and methods

2.1. Raw materials

The characteristics of the raw materials and their source are listed in Table 1.

2.2. Determination of the optimum Fe_2O_3 ratio

The selection of the optimum Fe_2O_3:Al ratio in this study is supported by established principles of thermite reaction kinetics and industrial welding practice. The thermite reaction between iron oxide and aluminum is known to proceed with adiabatic temperatures frequently exceeding 3000 K, ensuring complete melting of the produced iron and facilitating proper weld formation [1, 3]. However, the reaction behavior is highly sensitive to the fuel-to-oxidizer ratio, as deviations from the stoichiometric balance can significantly affect the energy release, reaction completeness, and weld quality [5, 8].

The observed reaction time of 26.43 s for the 3:1 ratio falls within the typical duration range for conventional thermite welding operations, where the exothermic reaction generally completes within several seconds to approximately 30 s [2, 6]. Comparable reaction times have been reported for standard rail thermite welding processes, confirming that the selected ratio yields a practically acceptable reaction rate [5, 8]. Furthermore, previous investigations have demonstrated that the Fe_2O_3-Al system exhibits distinct exothermic stages and that the overall reaction kinetics are influenced by factors such as particle size, mixing homogeneity, and initial temperature [9, 10]. The relatively rapid yet controlled reaction observed at the 3:1 ratio in the present work is consistent with these kinetic characteristics and aligns with the industrial preference for a reaction time that balances sufficient heat generation with manageable casting conditions [4, 6]. These comparisons confirm that the selected 3:1 ratio and the resulting reaction time of 26.43 s are appropriate and consistent with both fundamental thermite reaction characteristics and established industrial practices.

2.3. Preparation of TiO_2-containing composites

Following identification of the optimum Fe_2O_3 ratio, TiO_2 nanoparticles were incorporated into the selected composition (3:1 ratio) at concentrations of 0.1, 0.2, 0.3, 0.4, and 0.5 wt%.

The powders were mixed in cyclohexane using ultrasonic agitation to promote homogeneous nanoparticle distribution. After drying, the resulting mixtures were used for subsequent sample fabrication.

Table 1. Raw material specifications.

Raw material	Purity (wt%)	Av. particle size	Supplier/source	Function/role
Iron(III) oxide (Fe_2O_3)	98.5%	350 μm	Local provider (Iran)	Primary oxidizer in the thermite reaction (source of oxygen and iron)
Aluminum (Al)	99.9%	450 μm	Local provider (Iran)	Metallic fuel and reducing agent in the thermite reaction
Titanium dioxide (TiO_2) nanoparticles	99.5%	50 nm	US Research Nanomaterials, Inc.	Reinforcing phase to promote the formation of FeTi/Fe_2Ti intermetallic compounds and improve mechanical properties

2.4. Preparation of bulk samples

Bulk samples were fabricated using sand molds. Approximately 200 g of each powder mixture was placed into the mold cavity, and the thermite reaction was initiated using a sparkler.

Following complete cooling, the solidified products were removed from the molds and cleaned. Preliminary experiments using alumina tubes resulted in thermal-shock-induced cracking; therefore, sand molds were employed throughout the experimental procedure.

2.5. Microstructural characterization

Phase identification was carried out using X-ray diffraction (XRD) analysis with a Philips PW1730 diffractometer employing Cu–Kα radiation.

Microstructural observations were conducted using field-emission scanning electron microscopy (FESEM, TESCAN MIRA3) equipped with an energy-dispersive spectroscopy (EDS) detector for elemental characterization.

2.6. Mechanical characterization

Vickers hardness measurements were performed according to ASTM E92 using a load of 10 kgf and a dwell time of 15 s. Tensile tests were carried out according to ASTM E8 at a crosshead speed of 5 mm/min, whereas compression tests were conducted according to ASTM E9. Charpy impact testing was performed according to ASTM E23. Wear behavior was evaluated using a pin-on-disk apparatus according to ASTM G99 under an applied load of 20 N and a rotational speed of 200 rpm.

All experiments were conducted at room temperature. At least three specimens were tested for each condition, and the obtained results are reported as mean ± standard deviation.

3. Results and discussion

3.1. Determination of the optimum Fe_2O_3 ratio

Prior to nanoparticle addition, the optimum Fe_2O_3 ratio was determined through measurements of reaction time and iron yield. The experimental results are summarized in Table 2. Among the investigated compositions, the Fe_2O_3 ratio of 3:1 exhibited the highest iron yield (116.22 g) together with a reaction time of 26.43 s, which lies within the desirable industrial range of 23–28 s [5]. Consequently, this composition was selected as the optimum ratio for subsequent experiments.

Table 2. Reaction time and iron yield for different Fe_2O_3 ratios.

Ratio	Reaction time(s)	Iron yield (g)
1:1	15.69±1.2	105.5
2:1	19.73±1.5	108.3
3:1	26.43±1.8	116.22
4:1	31.24±2.1	110.5

3.2. Phase analysis by XRD

X-ray diffraction patterns obtained for the base sample (0 wt% TiO_2) and the sample containing 0.3 wt% TiO_2 are presented in Fig. 2. The diffraction pattern of the base sample reveals dominant peaks corresponding to α-Fe and α-Al_2O_3 phases. In addition, a relatively weak peak is observed at approximately 37.5 °, indicates the presence of γ-Al_2O_3, which may be associated with localized rapid cooling conditions during solidification [20].

Following TiO_2 nanoparticle incorporation, additional diffraction peaks appear. A peak at approximately 25.4 ° corresponds to anatase TiO_2. Furthermore, peaks observed at approximately 35.4 ° and within the range of 50–52 ° are attributed to FeTi and Fe_2Ti intermetallic phases, respectively [21, 22]. The TiO_2-containing sample also exhibits slightly increased α-Al_2O_3 peak intensity together with broadening of the Fe (110) diffraction peak at 44.7 °. Such peak broadening is commonly associated with grain refinement and residual lattice strain within the material.

3.3. Density and hardness

Density measurements exhibited a progressive increase from 6.42 g/cm^3 for the base sample to a maximum of 7.81 g/cm^3 at 0.4 wt% TiO_2, corresponding to a 21.7% improvement, followed by a slight reduction to 7.78 g/cm^3 at 0.5 wt%. This notable densification cannot be attributed simply to the addition of lower-density TiO_2 (~4.23 g/cm^3), but rather to the in-situ formation of high-density FeTi and Fe_2Ti intermetallic phases (6.5–6.7 g/cm^3) during the thermite reaction. These intermetallic compounds effectively fill the interdendritic shrinkage porosities and micro-voids inherently present in cast iron structures. Concurrently, the uniformly dispersed nanoparticles and the resulting intermetallic particles act as heterogeneous nucleation sites, promoting grain refinement that minimizes large void formation during rapid solidification. The slight density decrease at 0.5 wt% signals the onset of nanoparticle agglomeration, where excessive surface energy drives particle clustering, trapping gas and impeding melt flow, thereby introducing localized porosity and non-uniform packing.

Fig. 1. Photograph showing cracking of an alumina tube mold due to thermal shock during thermite reaction.

Hardness followed a remarkably similar trend, increasing from 215 HV in the base sample to a peak of 293 HV at 0.4 wt% TiO_2 (a 36.3% enhancement), before declining to 284 HV at 0.5 wt%. This improvement arises from the synergistic activation of multiple strengthening mechanisms. First, the uniform dispersion of hard TiO_2 nanoparticles and FeTi/Fe_2Ti intermetallic particles acts as formidable obstacles against dislocation motion through the Orowan strengthening mechanism, where the minimized interparticle spacing at optimal concentrations substantially increases the stress required for dislocations to bypass these barriers. Second, the refined grain structure, resulting from enhanced heterogeneous nucleation, contributes through the Hall–Petch relationship, where the increased density of grain boundaries effectively impedes dislocation slip. Third, the coefficient of thermal expansion mismatch between the iron matrix (~11.8 × 10^{-6} K^{-1}) and the reinforcing phases induces significant thermal residual stresses during rapid cooling, generating a high density of geometrically necessary dislocations around particles, thereby inducing localized work hardening. Fourth, the reduced porosity ensures that the applied load is efficiently transferred through a continuous, pore-free matrix to the reinforcing phases, enhancing the overall resistance to indentation. The sharp decline at 0.5 wt% directly confirms the detrimental agglomeration effect, where nanoparticle clusters cease to act as discrete reinforcing obstacles and instead create stress-concentrating regions and weak interfacial boundaries that easily deform or fracture under load. The strong correspondence between the density and hardness curves validates that structural homogeneity is the essential precondition for effective strengthening, with the maximum performance achieved at the threshold where the highest volume fraction of uniformly dispersed particles is obtained (0.4 wt%), beyond which the system becomes supersaturated and susceptible to clustering.

3.4. Microstructural characterization by SEM–EDS

SEM micrographs (Fig. 3a) revealed a two-phase microstructure consisting of a bright matrix region and darker secondary-phase regions. Based on the contrast observed in backscattered electron (BSE) images, the bright regions were identified as iron-rich areas, whereas the darker regions corresponded to titanium-rich phases.

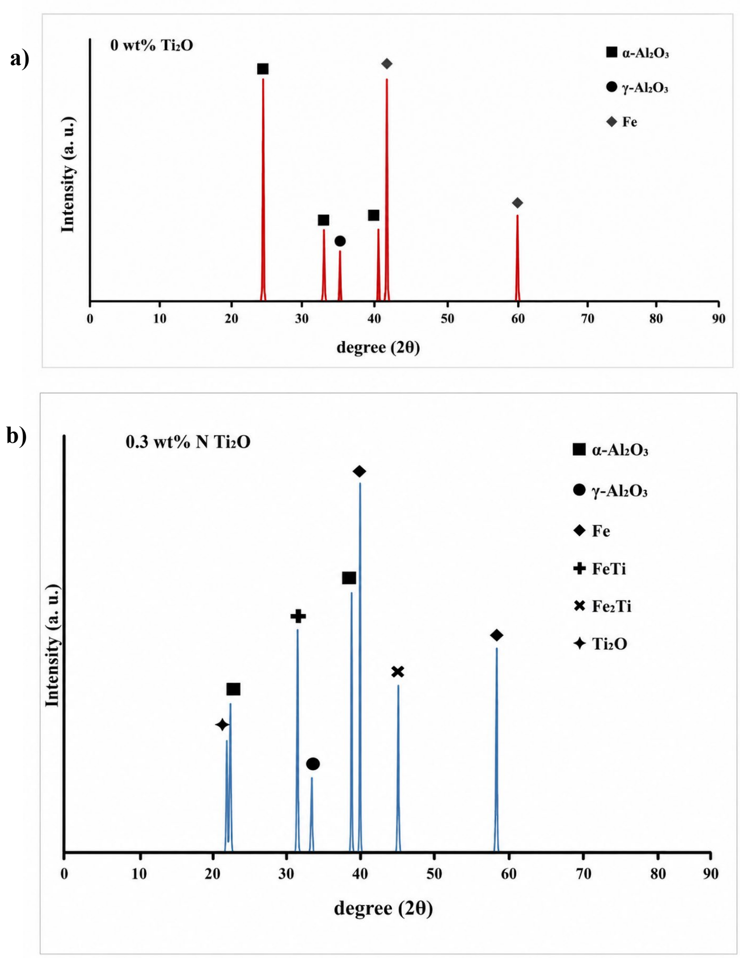

Fig. 2. XRD patterns of a) base sample (0 wt% TiO_2) and b) sample containing 0.3 wt% TiO_2 nanoparticles. Peaks corresponding to FeTi and Fe_2Ti intermetallic phases appear in b.

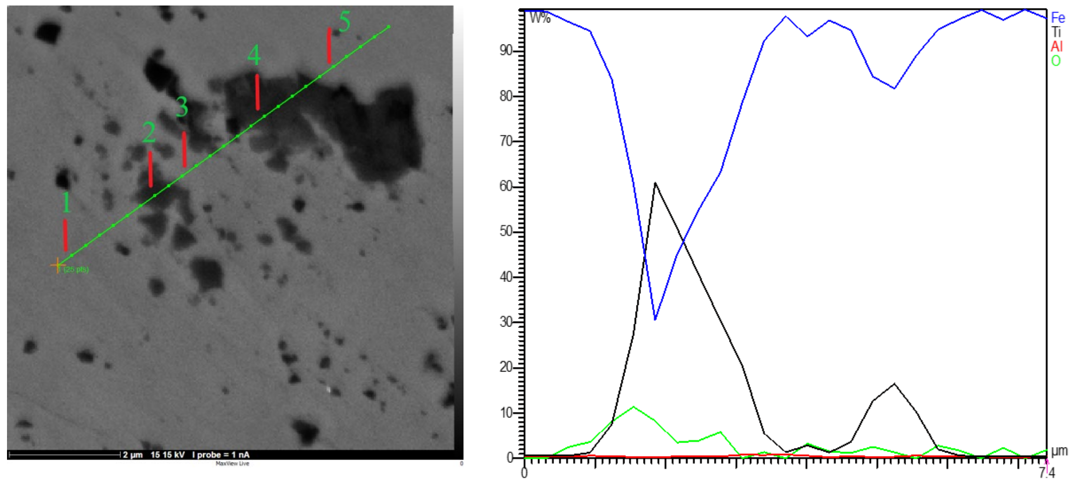

Fig. 3. a) Backscattered electron FESEM image of the sample with 0.3 wt% TiO_2 nanoparticles showing bright (Fe-rich) and dark (Ti-rich) regions, and b) corresponding EDS line scan showing elemental distribution across the interface.

EDS line-scan analysis (Fig. 3b) further confirmed this elemental distribution. The bright regions exhibited high iron concentrations, while elevated titanium contents were detected in the darker regions.

To identify the phases more accurately, point EDS analyses were conducted at the locations indicated in Fig. 4, and the obtained results are summarized in Table 3. Point 1 contained approximately 98.81 wt% Fe and was therefore identified as the α-Fe phase. Point 2, located within a darker region, contained 45.06 wt% Fe and 50.94 wt% Ti, corresponding closely to the stoichiometric composition of the FeTi intermetallic phase. Point 3 was similarly identified as α-Fe because of its high iron content. Point 4 exhibited elemental concentrations of 72.81 wt% Fe and 26.12 wt% Ti, which are consistent with the Fe_2Ti intermetallic phase. Point 5 was also identified as α-Fe.

The simultaneous presence of FeTi and Fe_2Ti intermetallic phases alongside the iron matrix indicates that TiO_2 nanoparticle addition promotes phase transformation reactions during the thermite process.

Elemental mapping results (Fig. 5) provide further insight into the distribution of elements throughout the microstructure. Titanium was primarily concentrated within regions corresponding to FeTi and Fe_2Ti intermetallic phases identified in SEM observations. In contrast, aluminum displayed a relatively homogeneous distribution throughout the matrix, predominantly existing as finely dispersed Al_2O_3 particles.

SEM images corresponding to different TiO_2 contents are presented in Fig. 6. At 0.2 wt% TiO_2 (Fig. 6a), the intermetallic particles are fine and uniformly distributed throughout the matrix. Increasing the TiO_2 content to 0.4 wt% (Fig. 5b) results in an increased particle volume fraction while maintaining uniform dispersion characteristics.

However, at 0.5 wt% TiO_2 (Fig. 5c), significant particle agglomeration becomes evident. This behavior can be attributed to the high surface energy of nanoparticles and increased particle interactions during both the mixing and thermite reaction stages [28]. Such agglomerates act as preferential nucleation sites for localized intermetallic phase formation, resulting in non-uniform particle distribution throughout the matrix.

3.5. Mechanical properties

Mechanical testing demonstrated that TiO_2 nanoparticle incorporation systematically enhances the performance of Fe_2O_3–Al reactive composites, with optimal properties achieved at 0.4 wt% followed by a decline at 0.5 wt% due to agglomeration. Tensile strength increased from 492 MPa (base) to 665 MPa at 0.4 wt% TiO_2 (35.2% improvement), while elongation also increased, indicating that strengthening was achieved without sacrificing ductility. Compressive strength rose from 617 MPa to 732 MPa (18.6% increase). The most significant enhancement was observed in Charpy impact energy, which increased from 164 J to 265 J (61.6% improvement). Wear resistance also improved considerably, with wear depth decreasing from 173 µm to 121 µm at a sliding distance of 721.9 m (30% reduction).

Table 3. EDS point analysis results corresponding to Fig. 3.

Point	Fe (wt%)	Ti (wt%)	Al (wt%)	O (wt%)	Identified phase
1	98.81	0.68	0.53	0	α-Fe
2	45.06	50.94	0.46	3.54	FeTi
3	97.76	1.76	1.38	0	α-Fe
4	72.81	26.12	0.37	0.82	Fe_2Ti
5	99.23	0.42	0.35	0	α-Fe

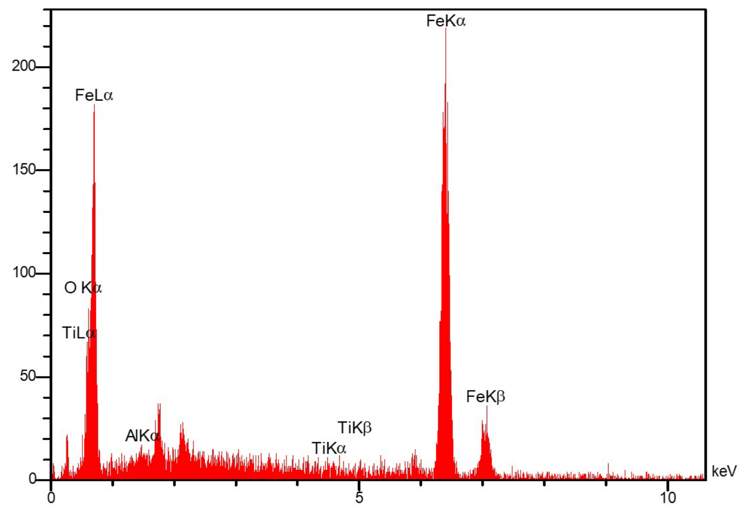

Fig. 4. EDS point analysis for the 0.3 wt% TiO_2 sample. The numbered points correspond to the analysis in Table 2.

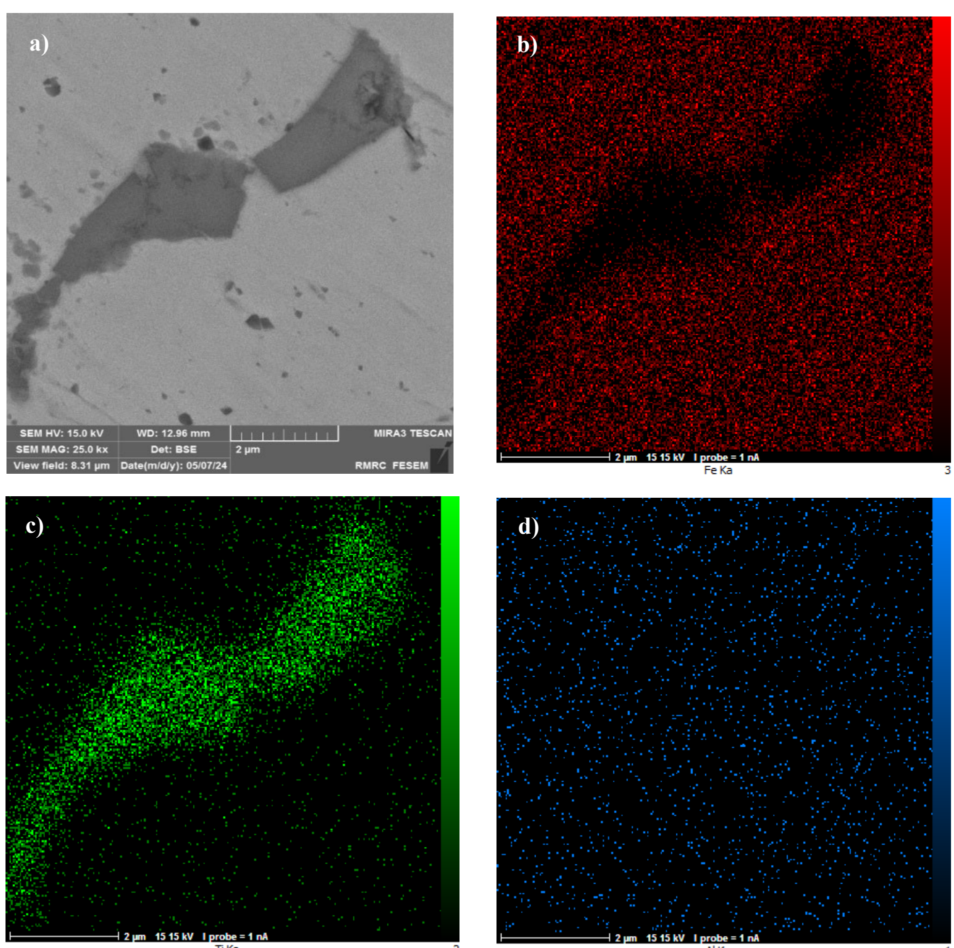

Fig. 5. Elemental mapping of the 0.3 wt% TiO_2 sample: a) SEM image, b) Fe Kα, c) Ti Kα, and d) Al Kα. Titanium is concentrated in isolated regions corresponding to intermetallic phases.

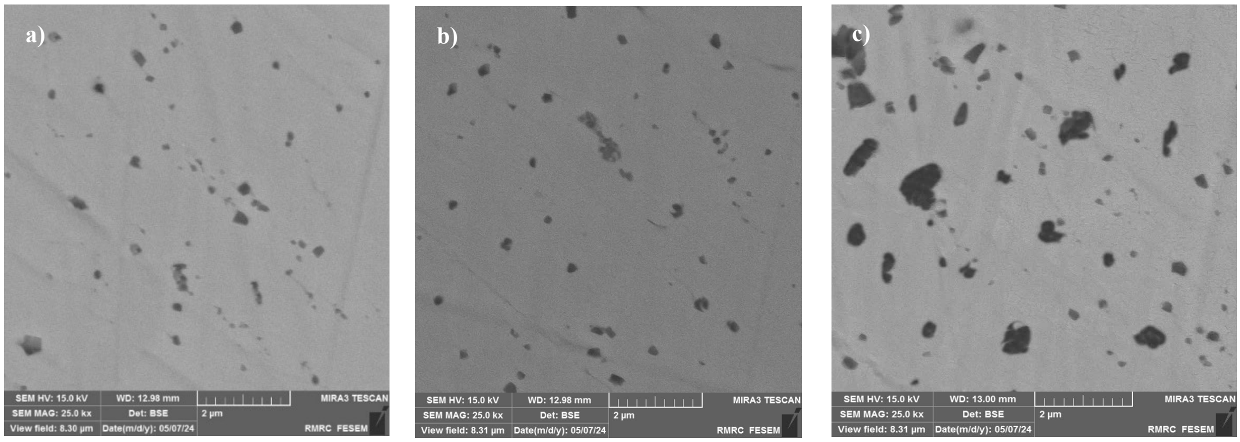

Fig. 6. FESEM images of samples with different TiO_2 nanoparticle contents: a) 0.2 wt%, b) 0.4 wt%, and c) 0.5 wt%. Uniform distribution is observed up to 0.4 wt%, while agglomeration is evident at 0.5 wt%.

EDS line-scan analysis (Fig. 3b) further confirmed this elemental distribution. The bright regions exhibited high iron concentrations, while elevated titanium contents were detected in the darker regions.

To identify the phases more accurately, point EDS analyses were conducted at the locations indicated in Fig. 4, and the obtained results are summarized in Table 3. Point 1 contained approximately 98.81 wt% Fe and was therefore identified as the α-Fe phase. Point 2, located within a darker region, contained 45.06 wt% Fe and 50.94 wt% Ti, corresponding closely to the stoichiometric composition of the FeTi intermetallic phase. Point 3 was similarly identified as α-Fe because of its high iron content. Point 4 exhibited elemental concentrations of 72.81 wt% Fe and 26.12 wt% Ti, which are consistent with the Fe_2Ti intermetallic phase. Point 5 was also identified as α-Fe.

The simultaneous presence of FeTi and Fe_2Ti intermetallic phases alongside the iron matrix indicates that TiO_2 nanoparticle addition promotes phase transformation reactions during the thermite process.

Elemental mapping results (Fig. 5) provide further insight into the distribution of elements throughout the microstructure. Titanium was primarily concentrated within regions corresponding to FeTi and Fe_2Ti intermetallic phases identified in SEM observations. In contrast, aluminum displayed a relatively homogeneous distribution throughout the matrix, predominantly existing as finely dispersed Al_2O_3 particles.

SEM images corresponding to different TiO_2 contents are presented in Fig. 6. At 0.2 wt% TiO_2 (Fig. 6a), the intermetallic particles are fine and uniformly distributed throughout the matrix. Increasing the TiO_2 content to 0.4 wt% (Fig. 6b) results in an increased particle volume fraction while maintaining uniform dispersion characteristics.

However, at 0.5 wt% TiO_2 (Fig. 6c), significant particle agglomeration becomes evident. This behavior can be attributed to the high surface energy of nanoparticles and increased particle interactions during both the mixing and thermite reaction stages [28]. Such agglomerates act as preferential nucleation sites for localized intermetallic phase formation, resulting in non-uniform particle distribution throughout the matrix.

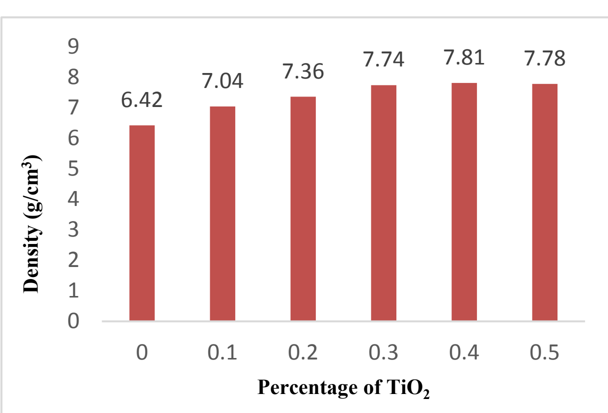

Fig. 7. Density of thermite composites as a function of TiO_2 nanoparticle content. Density increases up to 0.4 wt% and then slightly decreases.

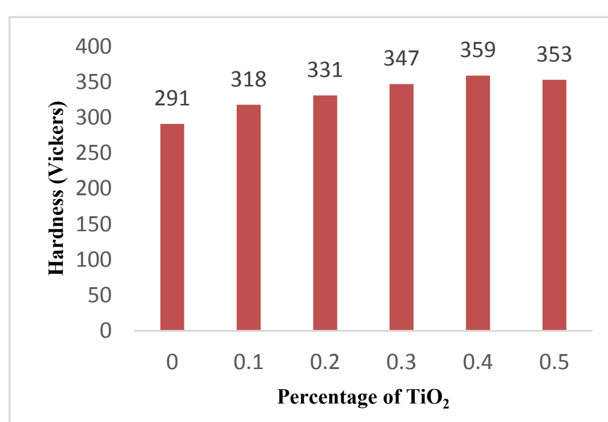

Fig. 8. Vickers hardness of samples with varying TiO_2 nanoparticle content. Hardness reaches a maximum at 0.4 wt%.

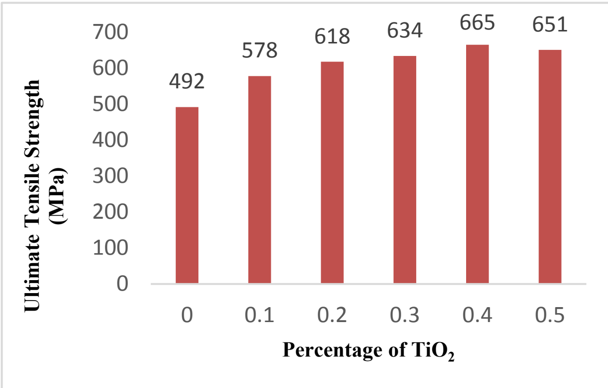

Fig. 9. Ultimate tensile strength of samples with different TiO_2 nanoparticle contents. The highest strength is achieved at 0.4 wt%.

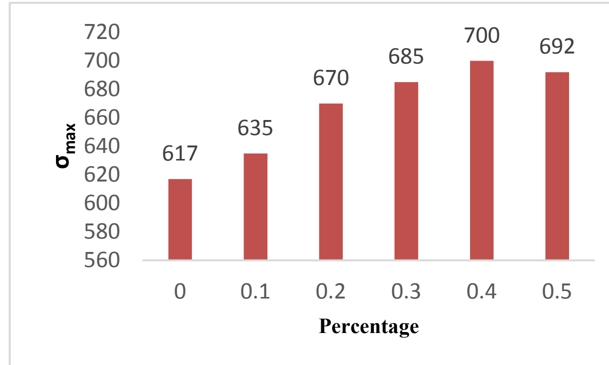

Fig. 10. Compressive strength of samples as a function of TiO_2 nanoparticle content. Maximum strength occurs at 0.4 wt%.

3.6. Mechanical properties

Mechanical testing demonstrated that TiO_2 nanoparticle incorporation systematically enhances the performance of Fe_2O_3–Al reactive composites, with optimal properties achieved at 0.4 wt% followed by a decline at 0.5 wt% due to agglomeration. Tensile strength increased from 492 MPa (base) to 665 MPa at 0.4 wt% TiO_2 (35.2% improvement), while elongation also increased, indicating that strengthening was achieved without sacrificing ductility. Compressive strength rose from 617 MPa to 732 MPa (18.6% increase). The most significant enhancement was observed in Charpy impact energy, which increased from 164 J to 265 J (61.6% improvement). Wear resistance also improved considerably, with wear depth decreasing from 173 µm to 121 µm at a sliding distance of 721.9 m (30% reduction).

These broad-spectrum improvements arise from the synergistic activation of multiple strengthening mechanisms [5, 6]. First, the uniform dispersion of hard TiO_2 nanoparticles and FeTi/Fe_2Ti intermetallic particles impedes dislocation motion through the Orowan strengthening mechanism [7, 8]. Second, the refined grain structure, resulting from enhanced heterogeneous nucleation, contributes through the Hall–Petch relationship [9]. Third, the coefficient of thermal expansion mismatch between the iron matrix and reinforcing phases generates thermal residual stresses and geometrically necessary dislocations around particles, inducing localized work hardening [5, 10]. Fourth, the reduced porosity ensures efficient load transfer from the matrix to the reinforcing phases [6, 8]. The decline in all properties at 0.5 wt% provides direct evidence of the detrimental agglomeration effect, where nanoparticle clusters create stress-concentrating regions and weak interfacial boundaries that act as preferential sites for crack initiation and propagation [9, 10]. The simultaneous improvement in strength, toughness, and wear resistance observed in this study is consistent with previous reports on nanoparticle-reinforced metallic systems [11, 12]. In summary, the optimum performance at 0.4 wt% TiO_2 represents the critical threshold where the highest volume fraction of uniformly dispersed reinforcing phases is obtained, ensuring maximum synergistic contribution from Orowan strengthening, grain refinement, load transfer, and crack deflection, while minimizing the adverse effects associated with nanoparticle clustering.

4. Discussion

The observed improvements in mechanical performance can be attributed to the combined contribution of several strengthening mechanisms acting simultaneously within the composite system.

First, FeTi and Fe_2Ti intermetallic particles together with residual TiO_2 nanoparticles can serve as heterogeneous nucleation sites during solidification, resulting in grain refinement [10]. According to the Hall–Petch relationship, decreasing grain size contributes directly to enhanced strength. Second, the dispersed FeTi and Fe_2Ti intermetallic particles impede dislocation motion and contribute to strengthening through the Orowan mechanism [24]. Since Orowan strengthening is inversely related to interparticle spacing, its contribution remains highly dependent on nanoparticle concentration and dispersion quality [25].

Third, hard intermetallic particles act as barriers against plastic deformation and bear a portion of the applied load, particularly under compressive loading conditions. Strong interfacial bonding between particles and the surrounding matrix facilitates effective stress transfer from the matrix to reinforcing particles [26]. Additionally, differences

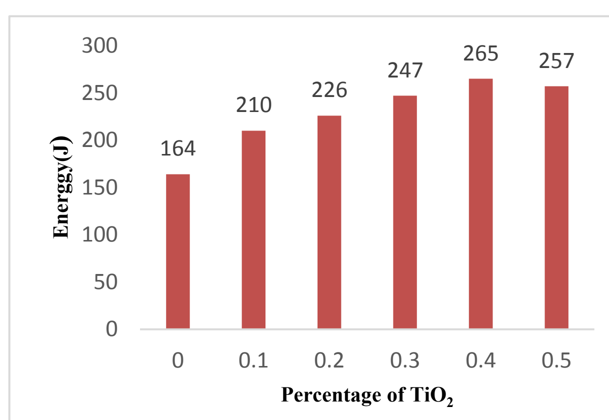

Fig. 11. Charpy impact energy absorbed by samples with different TiO_2 nanoparticle contents. Impact toughness increases dramatically up to 0.4 wt%.

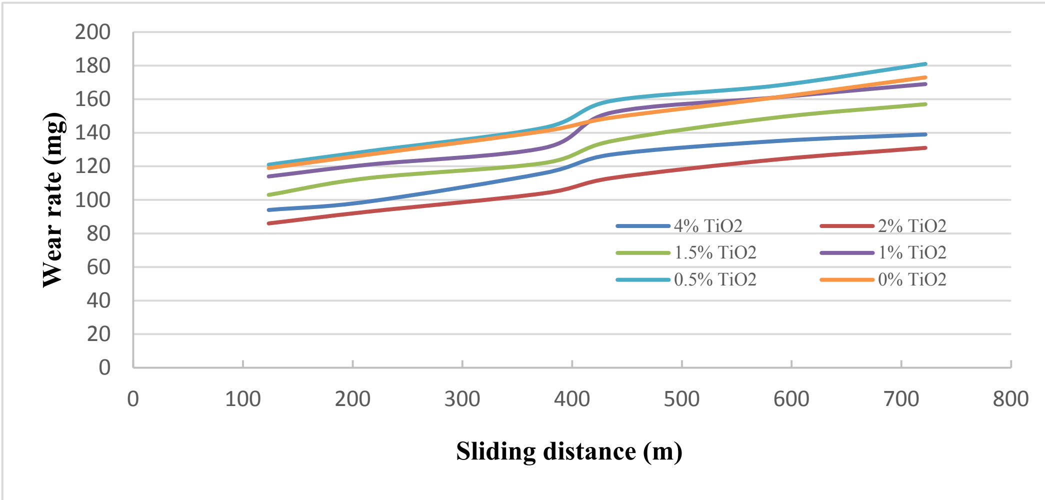

Fig. 12. Wear depth versus sliding distance for samples with various TiO_2 nanoparticle contents. The 0.4 wt% sample exhibits the lowest wear depth throughout the test.

in thermal expansion coefficients generate thermal stresses and introduce additional dislocations around reinforcing particles, thereby increasing dislocation density [27].

The substantial increase in impact energy observed in the present work indicates that intermetallic particles not only improve strength but also contribute significantly to toughness enhancement through crack deflection and advanced fracture dynamics [24, 28].

The present results are generally consistent with previous studies on nanoparticle-reinforced metallic systems. Fattahi et al. [13] reported improvements of approximately 30% in tensile strength and 35% in hardness following TiC nanoparticle addition to aluminum welds, which are comparable to the findings of the present study. Ramkumar and Natarajan [11] similarly observed enhancements of approximately 25% in tensile strength and 30% in hardness following TiO_2 nanoparticle incorporation.

However, the improvement in impact energy observed in the present work exceeds values commonly reported in the literature. This behavior may be attributed to the unique characteristics of thermite processing, including extremely high reaction temperatures and rapid solidification rates, which may enhance the interfacial bonding between intermetallic particles and the matrix.

Based on the overall evaluation of mechanical properties, the optimum TiO_2 content was identified as 0.4 wt%. At this concentration, the material exhibited maximum density, hardness, tensile strength, compressive strength, impact energy, and wear resistance. Although the sample containing 0.3 wt% TiO_2 also demonstrated excellent performance and may represent a safer choice for minimizing agglomeration risk, the experimental results indicate that 0.4 wt% provides the best overall performance under the processing conditions employed in this study.

5. Conclusions

The effect of TiO_2 nanoparticle addition on the microstructure and mechanical properties of Fe_2O_3–Al reactive composites was systematically investigated. The following conclusions can be drawn:

- The optimum Fe_2O_3 ratio was identified as 3:1, yielding the highest iron production (116.22 g) with a reaction time of 26.43 s, which falls within the desirable industrial range of 23–28 s.
- TiO_2 nanoparticle incorporation promoted the formation of FeTi and Fe_2Ti intermetallic phases within the iron matrix. Uniform particle distribution was achieved up to 0.4 wt%, whereas noticeable agglomeration occurred at 0.5 wt%.
- Mechanical properties improved significantly with TiO_2 addition. The sample containing 0.4 wt% TiO_2 exhibited the highest overall performance, including increases of 36.3% in hardness, 35.2% in tensile strength, and 21.7% in density relative to the base sample. Furthermore, impact energy increased by 61.6%, while wear depth decreased by approximately 30%.
- The simultaneous enhancement of strength and toughness was attributed to multiple strengthening mechanisms, including Hall-Petch grain refinement, Orowan strengthening induced by FeTi/Fe_2Ti intermetallic particles, crack deflection mechanisms, and thermal mismatch effects.
- The results demonstrate that the incorporation of optimum TiO_2 nanoparticle concentrations (0.3–0.4 wt%) represents an effective strategy for simultaneously improving strength and toughness in iron-based thermite composites.

What's next?

The findings of this study open up several promising avenues for future research and industrial application. The successful integration of TiO_2 nanoparticles into the Fe_2O_3–Al thermite system provides a practical pathway for producing high-strength, wear-resistant iron-based composites using a relatively simple and cost-effective ultrasonic mixing approach. This method can be readily scaled up for in-situ welding applications in railway maintenance and military equipment manufacturing, where access to sophisticated production facilities is often limited.

However, further investigations are required to optimize the processing parameters, such as ultrasonic mixing time, nanoparticle dispersion techniques, and cooling rates during solidification. Additionally, exploring the synergistic effects of combining TiO_2

with other ceramic nanoparticles (e.g., ZrO_2, SiC, or TiC) or incorporating rare-earth elements could potentially yield even greater improvements in mechanical properties and high-temperature performance. The role of residual oxygen and its interaction with the intermetallic phases also warrants deeper examination using in-situ characterization techniques.

CRediT authorship contribution statement

Mostafa Pasban: Conceptualization, Methodology, Investigation, Data curation, Formal analysis, Writing – original draft.
Ali Alizadeh: Supervision, Validation, Writing – review & editing.
Hamid Reza Baharvandi: Supervision, Writing – review & editing.

Data availability

The data underlying this article will be shared on reasonable request to the corresponding author.

Declaration of competing interest

The authors declare no competing interests.

Funding and acknowledgment

This research did not receive any specific grant from funding agencies in the public, commercial, or not-for-profit sectors.
The authors would like to express their sincere appreciation to the research laboratory staff of Malek Ashtar University of Technology for their valuable technical assistance and support during the experimental work.

Declaration of generative AI and AI-Assisted technologies in the writing process

During the preparation of this manuscript, the authors used Grammarly and ChatGPT to improve language quality and perform grammar checking. Following the use of these tools, the authors carefully reviewed, revised, and edited the manuscript and assume full responsibility for the content of the published work.

References

[1] M.E. Molefe, J.-R. Tapamo, Classification of thermite welding defects using local binary patterns and k-nearest neighbors, Proceedings of the 2021 Conference on Information Communications Technology and Society (ICTAS), IEEE. (2021) 91–96. https://doi.org/10.1109/ICTAS50802.2021.9395030.

[2] C. Lonsdale, M. Engineer, Thermite Rail Welding: History, Process Developments, Current Practices and Outlook for the 21st Century, Proceedings of the AREMA Annual Conference. 1895 (1999) 18.

[3] N.A. Kozyrev, O.A. Kozyreva, A.A. Usoltsev, R.E. Kryukov, R.A. Shevchenko, Modern methods of rail welding, IOP Conf. Ser.: Mater. Sci. Eng. 253 (2017) 012002. https://doi.org/10.1088/1757-899X/253/1/012002.

[4] H. Farhangi, S.M. Mousavizadeh, Horizontal split-web fractures of flash-butt welded rails, Proceedings of the 8th International Fracture Conference. (2007) 509–517.

[5] G. Webster, R. Wimpory, Polycrystalline materials—Determination of residual stresses by neutron diffraction, ISO/TTA3 Technology Trends Assessment, Geneva, Switzerland. (2001).

[6] C. Lonsdale, J. Lewandowski, Fracture toughness of thermite rail weld steel, in: Proceedings of the 39th Mechanical Working and Steel Processing Conference, Iron and Steel Society/AIME. (1998) 1083–1090.

[7] T.I. Nazarova, A.A. Popov, S.V. Kuzmin, I.V. Ivanov, Study of microstructure and mechanical properties of Ti–45Al–(Fe,Nb) alloys, Intermetallics. 82 (2017) 26–31. https://doi.org/10.1016/j.intermet.2016.11.001.

[8] A. Skyttebol, B.L. Josefson, J.W. Ringsberg, Fatigue crack growth in welded rails under the influence of residual stresses, Eng. Fract. Mech. 72 (2005) 271–285. https://doi.org/10.1016/j.engfracmech.2004.04.006.

[9] A. Van der Heijden, Developments and challenges in the manufacturing, characterization and scale-up of energetic nanomaterials: A review, Chem. Eng. J. 350 (2018) 939–948. https://doi.org/10.1016/j.cej.2018.06.044.

[10] J.A. Puszynski, C.J. Bulian, J.J. Swiatkiewicz, Processing and ignition characteristics of aluminum–bismuth trioxide nanothermite systems, J. Propuls. Power. 23 (2007) 698–706. https://doi.org/10.2514/1.24989.

[11] K. Ramkumar, S. Natarajan, Investigations on microstructure and mechanical properties of TiO2 nanoparticle addition in Al3003 alloy joints by gas tungsten arc welding, Mater. Sci. Eng. A. 727 (2018) 51–60. https://doi.org/10.1016/j.msea.2018.04.091.

[12] W. Bo, S.B. Xue, Y.L. Han, Z.Q. Lin, Effect of combinative addition of Ti and Sr on modification of AA4043 welding wire and mechanical properties of AA6082 welded by TIG welding, Trans. Nonferrous Met. Soc. China. 27 (2017) 272–281. https://doi.org/10.1016/S1003-6326(17)60032-4.

[13] M. Fattahi, M. Mohammady, N. Sajjadi, M. Honarmand, Y. Fattahi, S. Akhavan, Effect of TiC nanoparticles on the microstructure and mechanical properties of gas tungsten arc welded aluminum joints, J. Mater. Process. Technol. 217 (2015) 21–29. https://doi.org/10.1016/j.jmatprotec.2014.10.022.

[14] D. Zhang, H. Terasaki, Y.I. Komizo, In situ observation of the formation of intragranular acicular ferrite at non-metallic inclusions in C–Mn steel, Acta Mater. 58 (2010) 1369–1378. https://doi.org/10.1016/j.actamat.2009.10.043.

[15] C.L. Yeh, W.C. Ke, Combustion Synthesis of TiB_2 and TiC in Self-Propagating High-Temperature Synthesis Mode, J. Alloys Compd. 509 (2011) 8375–8380. https://doi.org/10.1016/j.jallcom.2011.05.095.

[16] R.T. Mousavian, M. Hajizamani, S. Sharafi, A. Hajipour, Effect of mechanical activation on the aluminothermic reduction of TiO2, J. Therm. Anal. Calorim. 126 (2016) 1331–1340. https://doi.org/10.1007/s10973-016-5640-1.

[17] V.I. Kobyakov, D.Y. Kovalev, Phase formation in the Fe–Ti system under self-propagating high-temperature synthesis conditions, Int. J. Self-Propag. High-Temp. Synth. 24 (2015) 101–108. https://doi.org/10.3103/S1061386215020077.

[18] X. Li, Y. Chen, Z. Zhang, Solid solution strengthening of ferrotitanium alloys, J. Mater. Sci. 55 (2020) 12456–12467. https://doi.org/10.1007/s10853-020-04983-4.

[19] A. Kumar, M. Chakraborty, Functionally Graded Al Alloy Matrix In-Situ Composites, Metall. Mater. Trans. A. 41 (2010) 242–249. https://doi.org/10.1007/s11661-009-0063-3.

[20] L. Wang, D. Luss, K.S. Martirosyan, The behavior of nanothermite reactions based on Bi2O3/Al, J. Appl. Phys. 110 (2011) 074311. https://doi.org/10.1063/1.3647775.

[21] A. Mashayekh, H.R. Baharvandi, Activation energy analysis in (Hf,W)B2 solid solutions, J. Mater. Eng. Perform. 29 (2020) 1234–1244. https://doi.org/10.1007/s11665-020-04721-0.

[22] JCPDS-ICDD, Powder Diffraction File, Card No. 00-019-0636 (FeTi).

[23] JCPDS-ICDD, Powder Diffraction File, Card No. 00-015-0337 (Fe2Ti).

[24] B. Feng, Y.C. Li, S.Z. Wu, H.X. Wang, Z.M. Tao, X. Fang, A Crack-Induced Initiation Mechanism of Al–PTFE Under Quasi-Static Compression and Investigation of Influencing Factors, Mater. Des. 108 (2016) 411–417. https://doi.org/10.1016/j.matdes.2016.06.119.

[25] J. Cai, H. Feng, Y. Zhou, The influence of metallic particle size on the mechanical properties of polytetrafluoroethylene–Al–W powder composites, Appl. Phys. Lett. 92 (2008) 031903. https://doi.org/10.1063/1.2837667.

[26] S.W. Dean, J.K. Potter, R.A. Yetter, T.J. Eden, V. Champagne, M. Trexler, Energetic intermetallic materials formed by cold spray, Intermetallics 43 (2013) 121–130. https://doi.org/10.1016/j.intermet.2013.07.018.

[27] D.T. Osborne, M.L. Pantoya, Effect of Al particle size on the thermal degradation of Al/Teflon mixtures, Combust. Sci. Technol. 179 (2007) 1467–1480.

[28] S. Elbasuney, M.G. Zaky, M. Radwan, R.P. Sahu, I.K. Puri, Synthesis of CuO nanocrystals supported on multiwall carbon nanotubes for nanothermite applications, J. Inorg. Organomet. Polym. Mater. 29 (2019) 1407–1416. https://doi.org/10.1007/s10904-019-01108-0.

[29] Q. Nguyen, C. Huang, M. Schoenitz, K.T. Sullivan, E.L. Dreizin, Nanocomposite thermite powders with improved flowability prepared by mechanical milling, Powder Technol. 327 (2018) 368–380. https://doi.org/10.1016/j.powtec.2017.12.093.